Molecular Therapy
Methods & Clinical Development
Original Article

Studying how administration route and dose regulates antibody generation against LNPs for mRNA delivery with single-particle resolution

Rasmus Münter,[1] Esben Christensen,[1] Thomas L. Andresen,[1] and Jannik B. Larsen[1]

[1]Biotherapeutic Engineering and Drug Targeting, Department of Health Technology, Technical University of Denmark (DTU), 2800 Kongens Lyngby, Denmark

Following the recent approval of both siRNA- and mRNA-based therapeutics, nucleic acid therapies are considered a game changer in medicine. Their envisioned widespread use for many therapeutic applications with an array of cellular target sites means that various administration routes will be employed. Concerns exist regarding adverse reactions against the lipid nanoparticles (LNPs) used for mRNA delivery, as PEG coatings on nanoparticles can induce severe antibody-mediated immune reactions, potentially being boosted by the inherently immunogenic nucleic acid cargo. While exhaustive information is available on how physicochemical features of nanoparticles affects immunogenicity, it remains unexplored how the fundamental choice of administration route regulates anti-particle immunity. Here, we directly compared antibody generation against PEGylated mRNA-carrying LNPs administered by the intravenous, intramuscular, or subcutaneous route, using a novel sophisticated assay capable of measuring antibody binding to authentic LNP surfaces with single-particle resolution. Intramuscular injections in mice were found to generate overall low and dose-independent levels of anti-LNP antibodies, while both intravenous and subcutaneous LNP injections generated substantial and highly dose-dependent levels. These findings demonstrate that before LNP-based mRNA medicines can be safely applied to new therapeutic applications, it will be crucial to carefully consider the choice of administration route.

INTRODUCTION

Biomaterials used within nanomedicine were, until recently, a group of therapeutics mainly used for delivery of cytotoxic drugs to cancer cells.[1] Due to the toxic cargo, immune reactions toward the nanoparticles were typically not observed, as immune cells taking up the particles were killed before initiating an immune response toward the particle.[2] With the recent advent, and promising aspects,[3–7] of lipid nanoparticles (LNPs) for delivery of siRNA and mRNA[8–11]—drug cargoes, which in contrast to chemotherapeutics, act by immune stimulation of cells[12]—adverse reactions toward the nanocarriers itself,[13–15] and allergic cross-reactivities toward components in the particles also used in other pharmaceutical products,[16] is becoming an increasing concern.[17] In the COVID-19 vaccine programs relying on mRNA vaccines, more than a billion doses of LNPs have been administered, and allergic responses to nanomedicines is hence no longer a problem only relevant to a small group of patients with a certain type of cancer, but a concern for the general population.[11,14]

Nanomedicines are often PEGylated to ensure stability during manufacturing, storage, and after injection into blood or tissue.[17] Indeed, the LNPs used in the COVID-19 vaccines are also stabilized by PEGylated lipids.[14] Exposure to PEGylated nanomedicines including LNPs is, however, known to result in generation of antibodies of the IgM and IgG class against the PEG coating on the nanocarrier.[18] Such antibodies cannot only give rise to reduced plasma stability and increased clearance of the nanocarriers,[19] but are also known to induce severe toxic pseudo-allergic reactions.[17,20–22] Exposure to PEGylated LNPs could therefore result in immunogenic cross-reactions toward other PEGylated therapeutics administered in the weeks following injection,[23] potentially leading to the second PEGylated therapeutic being less effective,[18,24] as well as the second exposure causing anaphylaxis.[16] Generation of anti-PEG antibodies is well studied for PEGylated liposomes injected intravenously,[19] but is only starting to be unraveled for LNPs used for intravenous injections[18,25] and intramuscularly injected vaccines.[26–30] With the circumstances required for generation of anti-LNP antibodies (ALAs) not being clear, it is evident that the field lacks a fundamental understanding of how formulation composition, dose, and injection route affects anti-LNP immunity, before we can safely expand the use of the mRNA-LNP technology to new therapeutic applications.

Here, we investigated the generation of ALAs of the IgG and IgM class, following injections of high or low doses of PEGylated mRNA-encapsulating LNPs into mice through the intravenous,

Received 10 November 2022; accepted 8 May 2023;
https://doi.org/10.1016/j.omtm.2023.05.008.

Correspondence: Thomas L. Andresen, Biotherapeutic Engineering and Drug Targeting, Department of Health Technology, Technical University of Denmark (DTU), 2800 Kongens Lyngby, Denmark.
E-mail: tlan@dtu.dk
Correspondence: Jannik B. Larsen, Biotherapeutic Engineering and Drug Targeting, Department of Health Technology, Technical University of Denmark (DTU), 2800 Kongens Lyngby, Denmark.
E-mail: jannla@dtu.dk

intramuscular, or subcutaneous routes. The blood plasma concentration of ALAs, measured 7 days after LNP exposure, was studied using a sensitive and accurate microscopy-based assay termed single-particle antibody measurement (SPAM) assay,[30] measuring the ALA binding to individual authentic LNPs. The assay—which is based on a previously published method for quantifying liposome opsonization[31]—eliminates sampling of non-specific signal and ensures that ALAs are quantified based on recognition of the authentic PEG geometry (taking into account, e.g., surface curvature, LNP zeta potential, membrane fluidity, and PEG-lipid surface density): both common issues with conventional methods such as ELISA and SPR. By comparing the three administration routes, we find that subcutaneous injections result in the highest concentrations of ALAs in a dose-dependent manner, indicating that caution should especially be taken if this administration route is used for PEGylated therapeutics. The second highest concentration of ALAs was quantified for intravenous injections with the previously reported inverse dose dependency.[32] Finally, intramuscular injections typically resulted in the lowest, although non-zero, amounts of ALAs compared with the other injection routes. Hence, anti-LNP immunogenicity should be carefully considered when applying LNP-based mRNA drugs to therapeutic areas beyond vaccination.

RESULTS

To study the generation of ALAs in response to PEGylated LNPs, we first prepared mRNA-encapsulating PEGylated LNPs. We used a standard LNP formulation consisting of the ionizable lipid DLin-MC3-DMA, cholesterol, DSPC, and the sheddable PEG lipid DMG-PEG2000 in a molar ratio of 50:38.5:10:1.5 (for LNP characteristics, see Table S1). Having successfully prepared the LNPs, these were then injected into mice at a dose of either 0.3 mg/kg mRNA or 0.0003 mg/kg mRNA. Injections were performed intravenously, subcutaneously, or intramuscularly. Intravenous injections are most commonly used for LNP-mediated cancer treatments, and delivery of siRNA to the liver,[9] and are also the most well studied for PEGylated nanoparticles in general.[17,22] Recently, intramuscular injections have become highly relevant in relation to mRNA-based therapeutics for vaccinations against, but not limited to,[3] COVID-19.[11] With those promising prospects of mRNA therapeutics, drug developers are investigating the effect of mRNA-carrying LNPs administered through alternative routes, including subcutaneous injections.[4,33] For all three administration routes blood samples were acquired 7 days after injection, followed by isolation of the blood plasma for determining the concentration of ALA (Figure 1A). A 7-day time point post injection is commonly used to study antibodies generated against LNPs[18,34] as the serum concentrations of such antibodies have been found to peak between days 5 and 10 in both rodents[35–37] and pigs.[38] The chosen study setup was hence relevant for expanding the current knowledge on anti-LNP immunity[18] to also include dose and administration route.

To study the ALA content in blood plasma we were inspired by a recently described microscopy-based methodology,[31] previously used for measuring plasma protein binding to individual liposomes. Here, we expanded the assay to facilitate the quantification of ALA binding to individual LNPs, hereby introducing a novel tool to study protein binding to LNPs with single-particle resolution and the ability to reveal inter-particle heterogeneity of LNP ensembles.[39,40] Typically, anti-PEG antibodies, generated in response to PEGylated LNPs, are measured using ELISAs where PEG lipids are adsorbed onto planar surfaces.[32] Such assays hence ignore the three-dimensional organization of the PEGs on the particle surface, the zeta potential of the particle, and the exact lipid mixture. Essentially such assays are trying to detect antibodies with a PEG array not resembling what the antibodies are actually generated against, and therefore the ELISA-based approach does not measure recognition of the exact antigen the antibodies will meet in the bloodstream upon later exposures. Alternatively, bulk assays based on isolation of nanoparticles from plasma using size or density separation may reflect binding to the actual particles, but are hampered by the high background amounts of protein aggregates and naturally occurring bionanoparticles.[41–44]

The SPAM assay used here, in contrast, allows for studying protein binding to authentic LNP surfaces while simultaneously eliminating most non-specific signals (Figure S1). This is done by immobilizing fluorescent DiI-labeled capturing LNPs on BSA-passivated glass surfaces, and incubating them with blood plasma (Figure 1B). After removing the plasma, fluorescently labeled AF488 antibodies against the protein of interest (in this case mouse IgM or IgG) are added to the sample. After a brief incubation, these detection antibodies are also removed, and the system is imaged using fluorescence confocal microscopy. In the images, LNPs appear like diffraction-limited spots (Figure 1C), and binding of IgM or IgG to the LNPs is determined using automated image analysis software. In brief, this analysis identifies all spots in both fluorescence channels of the images and then extracts the integrated intensity of each individual spot if this is above a specific threshold (Figure S2). Through spatial co-localization, the matching spots in the DiI and AF488 channels is used to identify specific ALA-LNP association, with DiI intensity correlating to the volume of the individual LNP (see Figure S3 for a description) and the AF488 intensity correlating with number of antibodies associated to that LNP (Figure 1D). By only including AF488 fluorescence co-localized with DiI spots in the analysis, background binding to the surface (see Figure S4 for details on this background) is effectively filtered out of the analysis, and only actual antibody-LNP interactions extracted from the data. We converted DiI intensity to LNP diameter (see Figure S3) and plotted the AF488 intensity as a function of LNP size, with each marker representing the measurement of an individual LNP (Figure 2). By comparing plasma samples from naïve mice (Figure 2A) with plasma samples from mice previously receiving intravenously dosed LNPs (Figure 2B), it was clear that both the number of LNPs adsorbing ALA, as well as the amount of ALA per LNP was increased. By studying plasma samples from mice that had received injections of LNPs through either the intravenous route (Figure 2B) or the subcutaneous route (Figure 2C), it was also evident that administration route affected the ALA concentration in the plasma samples, and thus the amount of ALA binding to the LNPs. Apart from this

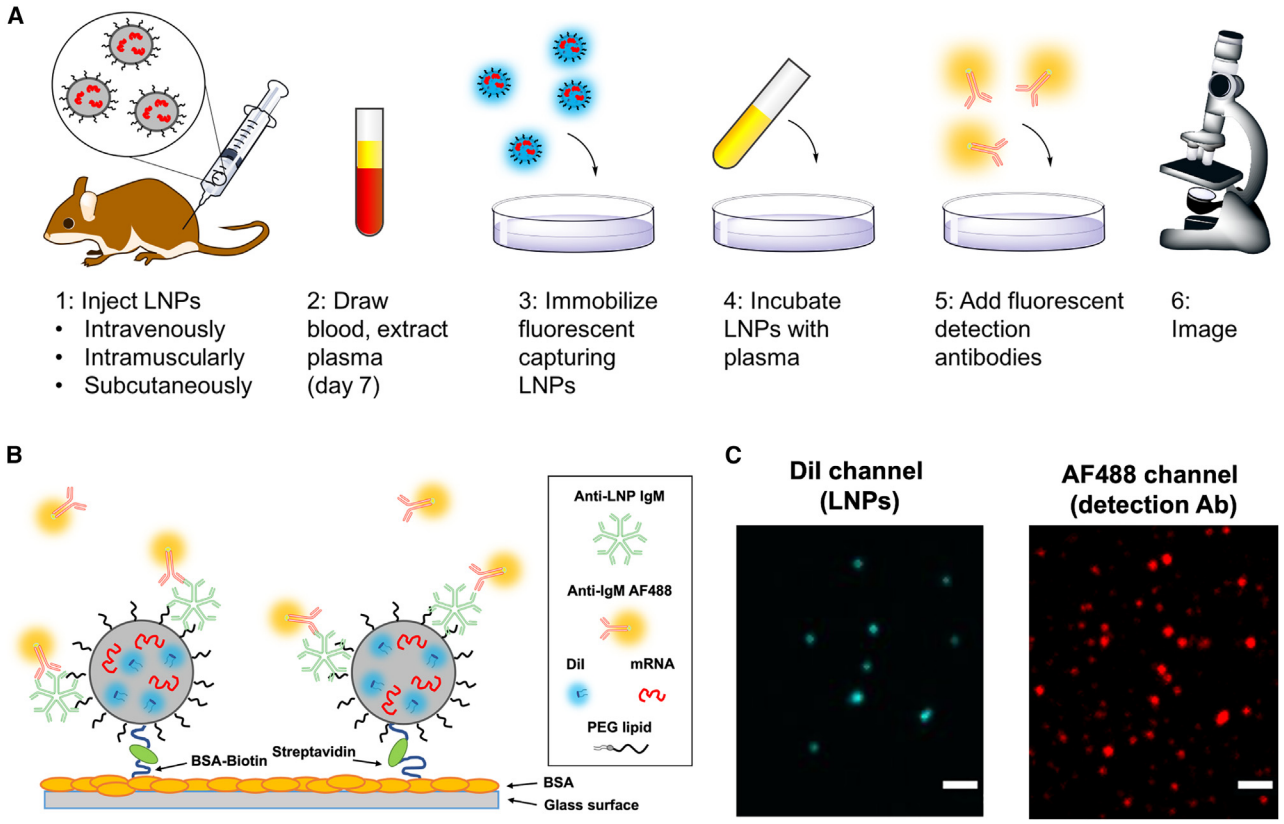

Figure 1. Assay for quantifying the binding of anti-LNP antibodies to authentic LNPs in blood plasma

(A) LNPs in either high (0.3 mg/kg) or low (0.0003 mg/kg) dose was injected intravenously (i.v.), subcutaneously (s.c.), or intramuscularly (i.m.) into mice. After 7 days, blood samples were drawn to analyze the blood concentration of anti-LNP IgM and IgG. This was done by immobilizing fluorescently labeled capturing LNPs in BSA-passivated microscopy slides (B), and incubating them first with blood plasma, then fluorescently labeled detection antibodies against either IgM or IgG, before imaging the system. (C) Confocal micrographs of individual LNPs imaged in the LNP channel (DiI, left) and LNP-associated ALAs in the detection antibody channel (AF488, right). Scale bar, 2 μm.

information about the fraction of LNPs in the ensemble being opsonized by antibodies, the single-particle nature of the assay also allows for studying how LNP size controls ALA binding (see, for example, Figure 2C). To facilitate a straightforward comparison of the generation of anti-LNP IgG and IgM for the different administration routes, we wanted to extract a single value, scaling with the total concentration of ALAs in the plasma sample, from each dataset. To this end, we plotted a histogram of all integrated intensity values for the ALA-LNP interactions in the sample (Figure 2D) and extracted the total ensemble binding of ALA by integrating the log-normal fit to the histogram. This total ensemble binding of ALA for all LNPs in one such sample, divided by the total number of LNPs in the ensemble, was used to extract the mean ALA fluorescence intensity (MFI_{ALA}) correlating to the average number of ALAs per LNP. In summary, we found that the assay was both capable of accurately measure ALA binding to individual LNPs and defined a value for reporting the average binding to all LNPs in the ensemble.

We first investigated the generation of ALAs in mice following injections of high doses (0.3 mg/kg) of mRNA-carrying LNPs. This dose mirrors what is used clinically for the siRNA-carrying drug Onpattro, and close to the commonly used mRNA doses administered in the literature.[45–49] The anti-LNP IgM intensity (MFI_{IgM}) in blood plasma samples following intravenous, subcutaneous, or intramuscular doses, compared with the baseline in untreated animals, is shown in Figure 3A. In blood plasma from mice receiving intravenous and intramuscular doses we quantified significantly 2-fold higher MFI_{IgM} levels compared with in the blood from untreated animals. After subcutaneous injections, the MFI_{IgM}, however, increased about 10-fold compared with in untreated animals, and more than 4-fold compared with intravenous or intramuscular injections. The single-particle resolution of the SPAM assay allowed us to also determine the percentage of LNPs in the ensemble being positive to the IgM. As shown in Figure S5, the majority of the LNPs were IgM positive in plasma from mice receiving LNPs subcutaneously, whereas the ALAs detected in plasma from animals receiving an intravenous of intramuscular injection were heterogeneously distributed among the LNPs in the assay, with only an average of 20% of the LNPs having detectable binding. While similar heterogeneity in protein adsorption has previously been shown for other nanoparticle types,[31,50] we here

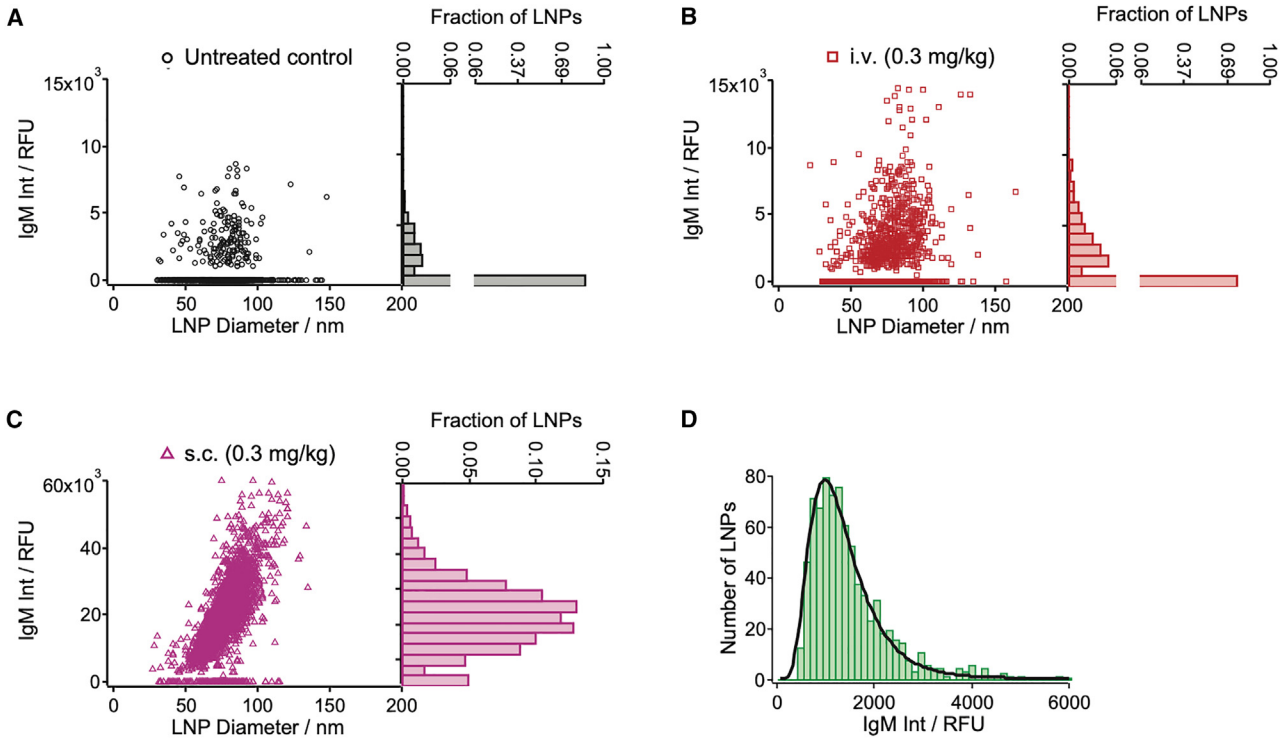

Figure 2. Co-localization analysis of ALA binding to individual LNPs

Co-localization analysis of the confocal micrographs with each dot representing the measurement of a single LNP. The horizontal axis shows the LNP diameter, and the vertical axis shows the integrated AF488 intensity (correlating with number of ALAs per LNP). (A) Untreated sample, (B) (0.3 mg/kg) intravenously dosed LNPs, (C) (0.3 mg/kg) subcutaneously dosed LNPs. (D) To calculate the INT_{ALA} value of a sample, a histogram of all ALA-positive LNPs in the measurement was plotted. The data in this histogram was fitted to a log-normal distribution (black curve). The mean of the log-normal distribution was then calculated. This mean value was divided by the total number of LNPs in the sample (both ALA positive and ALA negative) to get the INT_{ALA} value for the sample.

show for the first time that this also pertains to clinically relevant LNPs. In conclusion, the experiment demonstrated that administration of high LNP doses (0.3 mg/kg mRNA) through the subcutaneous route leads to a significantly higher generation of anti-LNP IgM than intravenous and intramuscular injections.

In addition to IgM, anti-PEG IgG has previously been found to be a main driver of allergic reactions against repeatedly intravenously dosed PEGylated liposomes,[21] and we therefore also measured the concentration of anti-LNP IgG following high doses of LNPs administered intravenously, subcutaneously, or intramuscularly (Figure 3B). The quantification of anti-LNP IgG per LNP in arbitrary intensity units (MFI_{IgG}) shows that MFI_{IgG} are lower than MFI_{IgM} across the different groups, potentially due to the pentameric structure of IgM compared with the monomeric structure of IgG. Only very low MFI_{IgG} values were measured in the plasma samples following intravenous and intramuscular administration, and thus the IgG adsorption to the capturing LNPs was not significantly higher than in plasma from untreated animals. Similar to what we observed for IgM, subcutaneous doses of LNPs led to a significant increase in plasma concentration of anti-LNP IgG, which was 11-fold higher than in untreated animals. In conclusion, high doses of subcutaneously administered LNPs will lead to a substantial generation of ALAs, giving a strong risk of generating antibodies that could potentially lead to immune reactions upon later exposure to PEGylated therapeutics. In addition, intravenous and intramuscular doses also lead to small but significant increase in ALAs, but only of the IgM class.

Generation of anti-PEG antibodies against intravenously administered PEGylated liposomes results in accelerated blood clearance (ABC) of a second liposome dose administered in the weeks following the first dose.[32] This ABC phenomenon is known to be inversely dose dependent, because a high dose of PEGylated nanoparticles leads to anergy of the marginal zone B cells in the spleen producing the anti-PEG antibodies and thus results in overall tolerance toward the PEGylated nanocarrier.[2,51] Therefore, we next investigated if a reduced dose of LNPs would lead to even higher generation of ALAs than what we observed for LNPs carrying 0.3 mg/kg mRNA. To do this, we reduced the dose by 1,000-fold to 0.0003 mg/kg (0.3 μg/kg), which resembles the dose at which the COVID-19 vaccines Spikevax and Comirnaty are administered (1.42 and 0.42 μg/kg, respectively, for an adult weighing 70 kg[14]). The anti-LNP IgM intensity (MFI_{IgM}) in blood plasma samples following intravenous, subcutaneous, or intramuscular doses, compared with the baseline in

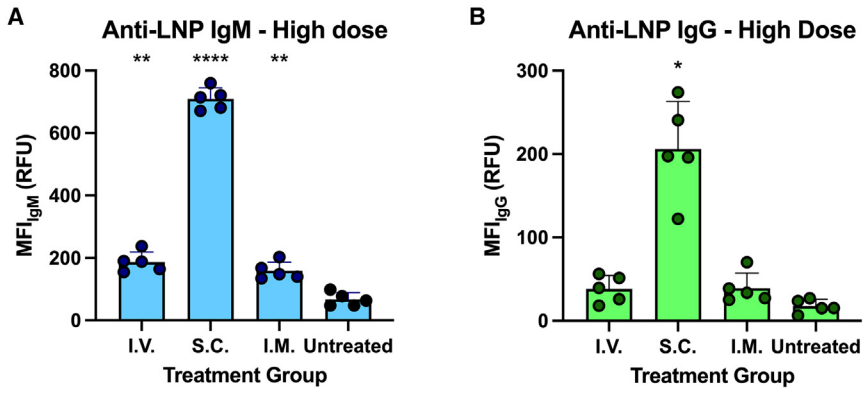

Figure 3. Blood plasma concentration of anti-LNP IgM and IgG depends on administration route

(A) Mean IgM AF488 fluorescence intensity (MFI_{IgM}) quantifying the IgM ALAs for LNPs administered at a high mRNA dose (0.3 mg/kg) through i.v., s.c., or i.m. administration. (B) Mean IgG AF488 fluorescence intensity (MFI_{IgG}) quantifying the IgG ALAs for LNPs administered at a high mRNA dose (0.3 mg/kg) through i.v., i.m., or s.c. administration. Each data point represents the measurement from a single mouse, each point of which corresponds to the average measured binding to at least 3,000 LNPs. N = 5. Bars show mean (SD). Statistics is based on a Brown-Forsythe and Welch ANOVA test with Dunnett's T3 adjustment for multiple comparisons, comparing each sample with the untreated control. *p > 0.05, **p > 0.005, ****p > 0.0001. Statistics are only shown for comparisons with the untreated control: other comparisons, and exact p values for all comparisons, are listed in Table S2.

untreated animals, is shown in Figure 4A. For intravenous injections, the MFI_{IgM} had increased approximately 3-fold compared with the high dose ($p = 0.0063$). In sharp contrast, the decrease in dose led to a 5-fold decrease in MFI_{IgM} for the subcutaneously dosed LNPs ($p = 0.0006$). For intramuscular injections, the MFI_{IgM} value displayed some variability for the five animals exposed to low LNP doses, but was neither significantly higher than the baseline value in untreated animals, nor different from what we observed for the high dose.

For the same plasma samples, we also quantified the concentration of anti-LNP IgG (Figure 4B). For low LNP doses administered intravenously, the MFI_{IgG} was highly variable, ranging from 37 to 276, with an average of 135. Similar to what we observed for IgM, there was thus also a trend toward an increase in anti-LNP IgG when decreasing the dose, as the high dose gave MFI_{IgG} values between 18 and 56. Following subcutaneous administrations of low LNP doses, the MFI_{IgG} was (apart from one sample) typically similar to the value found in plasma from untreated animals, and thus dramatically decreased compared with the high LNP doses. The MFI_{IgG} for low intramuscular LNP doses was similar to what we observed for the high doses and to what we measured in plasma from untreated mice. In conclusion, a reduction of the LNP dose leads to a strong increase in ALAs for intravenous administration, a remarkable decrease in ALAs for subcutaneous administration, while ALA generation following intramuscular injections was dose independent and remained low.

DISCUSSION

Nanomedicines were until recently a group of therapeutics mainly used for delivery of cytotoxic drugs to cancer cells.[1] Decades of research has therefore investigated how intravenously dosed liposomes interact with the immune system.[52] With the advent of mRNA therapeutics for vaccinations, new types of LNPs with other cargoes are now being developed. Investigating the effect of administration route and dose is thus of particular interest for LNPs, as low doses administered intramuscularly have proven to be relatively safe when applied for COVID-19 vaccines.[14,53] However, LNPs may in the near future be applied to many other therapeutic areas, where alternative doses and administration routes are used.[3–7] Since administration route determines the lymphoid organs taking up the particles, with different mechanisms being observed in spleen and lymph nodes for antibody responses toward polymeric particles[37] administration route may emerge as a key regulator of ALA generation.[41] The dose concentration may be of particular importance too, as differences in this have been proposed to be the cause for higher antibody generation toward the Moderna vaccine Spikevax compared with the Pfizer/BioNTech vaccine Comirnaty.[54] These new technologies have many exciting applications,[4] but rather than assuming that previously learned lessons can be applied to these new platforms,[14] the limitations and safety issues need to be closely investigated for any new use of the technology.

In this work, we report that the amount of ALAs increases with dose following subcutaneously injection of LNPs, which is in sharp contrast to the inverse dose dependence observed for intravenous injections both here and in previous studies on PEGylated liposomes.[32] We propose that the reason for the high amounts of ALAs generated following subcutaneous injections is because the drug depot created upon subcutaneous injections slowly releases LNPs into blood circulation.[55,56] Effectively, this will result in a low blood concentration of LNPs, leading to a similar antibody generation as for low intravenous LNP doses. Lack of control for this administration route is well known in rodents,[55] explaining the high variability we observed for the low doses. Rather than intact LNPs escaping from the subcutaneous depot into the blood, PEG lipids could also reach blood circulation by dissociating from the LNPs and associating to proteins or bionanoparticles.[57] Supporting this scenario is the fact that clinically approved LNPs use PEG lipids with short acyl chains, resulting in quick shedding from the LNP surface, allowing the particle to be efficiently internalized and escaping the endosome with the RNA cargo.[58,59] The observations for subcutaneous injections pinpoints a potential issue with subcutaneously administered LNPs, as anti-PEG immunity cannot be circumvented by increasing the dose, which should give precautions for researchers attempting to design therapeutics for such systems and administration routes. The different

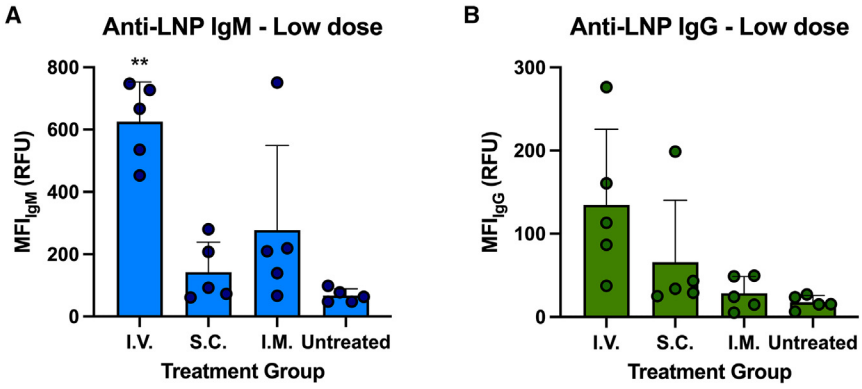

Figure 4. Blood plasma concentration of anti-LNP IgM and IgG depends on administration route

(A) Mean IgM AF488 fluorescence intensity (MFI_{IgM}) quantifying the IgM ALAs for LNPs administered at a low mRNA dose (0.0003 mg/kg) through i.v., s.c., or i.m. administration. (B) Mean IgM AF488 fluorescence intensity (MFI_{IgG}) quantifying the IgG ALAs for LNPs administered at a low mRNA dose (0.0003 mg/kg) through i.v., s.c., or i.m. administration. Each data point represents the measurement from a single mouse, each point of which corresponds to the average measured binding to at least 3,000 LNPs. N = 5. Bars show mean (SD). Statistics is based on a Brown-Forsythe and Welch ANOVA test with Dunnett's T3 adjustment for multiple comparisons comparing each sample with the untreated control. *p > 0.05, **p > 0.005, ****p > 0.0001. Statistics are only shown for comparisons to the untreated control: other comparisons and exact p values for all comparisons, are listed in Table S2.

dose-dependent results obtained for intravenous and subcutaneous administrations underpins how lessons learned from one administration route cannot be assumed to apply to another administration route.

For intramuscular LNP injections, under some circumstances we did observe a significant increase in ALA generation compared with untreated mice. Typically, however, intramuscular injections led to ALA concentrations similar to or lower than intravenous or subcutaneous injections, and remained low irrespective of the dose. This type of injection may therefore be considered safer with respect to anti-LNP immunity, compared with the other tested administration routes. Despite this, it has been reported recently that subjects vaccinated with the Moderna COVID-19 vaccine (Spikevax) have increased plasma concentrations of anti-PEG antibodies,[26,27] and that these antibodies can mediate increased neutrophil clearance of PEGylated therapeutics.[26] Indeed, recent studies have demonstrated mRNA transfection in the liver following intramuscular injections of FLuc-carrying LNPs,[60] indicating that LNPs do escape from the muscle into the bloodstream. It is, however, unclear why the ALA generation for this administration route differs so remarkably from both the intravenous and subcutaneous routes. Irrespective of the underlying mechanism, and despite most likely being a matter of tradition rather than a matter of avoiding anti-LNP immunity,[61] the intramuscular route used for administration of COVID-19 mRNA vaccines seems to have been a wise choice with respect to limiting ALA generation, despite reports of improved vaccine efficacy following subcutaneous administration.[62]

We studied the ALA generation inspired by a recently developed technique,[31] allowing investigations of protein binding to authentic LNP surfaces, taking into account the exact surface curvature, PEG density, zeta potential, and stiffness of the drug delivery vehicle in question. Whereas classical ELISAs, where an antigen such as the PEG lipid is immobilized onto a planar surface, cannot accurately reflect the binding scenario to an actual LNP surface, ELISAs have been developed where whole LNPs are immobilized in ELISA wells.[27,29] Our microscopy images, however, clearly show significant background binding to the surface (Figures 1C, S1, and S4), which would most likely require blocking to prevent or harsh washing to remove, potentially affecting the integrity of the immobilized LNPs and/or resulting in detachment of the detection LNPs. The herein presented methodology instead allows for gentle washing, and furthermore extraction of the background signal in a sample-specific manner, rather than measuring the background in a separate sample. In addition, when using confocal microscopy for detecting binding, the assay gains single-particle resolution, allowing for detecting both ALA-positive and ALA-negative LNPs in the same ensemble (Figures 2, S1, and S5). The underlying reason for this binding heterogeneity is currently unknown, but could be related to inhomogeneity in PEG density or surface charge of the individual LNPs in the sample. A drawback of the assay is, however, that the exact component of the LNP formulation being responsible for the ALA generation is not confirmed. As the part of the LNP "seen" by the surrounding environment will mainly be PEG, it will most likely be the PEG lipid, which is the exact antigen of the LNP, which is supported by reports on cross-interactions between ALAs and PEGylated liposomes,[26] hypersensitivity reactions to PEG-based bowel cleansing agents following vaccination with Spikevax,[16] and impaired circulation properties of PEGylated hemophilia medicine following vaccination with Comirnaty.[24] As patients developing hypersensitivity reactions to LNPs and PEGylated liposomes do not respond to non-conjugated PEG, the recognition seems to be highly context dependent.[63] Overall, this supports the necessity of distinguishing between anti-PEG antibodies and ALAs, with studies on the latter requiring a methodology as the one presented in this work.

Conclusion

Generation of antibodies against LNPs carrying mRNA was studied following injections of such LNPs through the intravenous, subcutaneous, or intramuscular route. High LNP doses administered intravenously and intramuscularly led to a small but significant increase in detectable ALAs, whereas subcutaneous administration resulted in very high levels of ALAs of both the IgG and IgM class, and significantly more than for the alternative administration routes investigated. While the ALA generation could be alleviated for

subcutaneous injections by decreasing the dose, the ALA generation following intravenous injections increased significantly when the dose was lowered. In contrast, intramuscular LNP injections only resulted in low amounts of ALAs being generated irrespective of the dose, indicating that this administration route is relatively safe with respect to anti-nanoparticle immunity upon repeated dosing, or cross-reactions with other therapeutics. Together, these findings highlight that anti-LNP immunogenicity needs to be investigated in detail, before the mRNA/LNP technology is applied for other therapeutic areas, requiring alternative administration routes and altered doses.

MATERIALS AND METHODS

Materials

EGFP-encoding mRNA (5-methoxy uridine modified and CleanCap capped) was acquired from TriLink (San Diego, CA). Ethanol, nuclease-free water, NaCl (10 M nuclease-free aqueous solution) and Triton X-100 was acquired from Merck/Sigma Aldrich (Darmstadt, Germany). (4-(2-Hydroxyethyl)-1-piperazineethanesulfonic acid) (HEPES) (1 M nuclease-free aqueous solution) was acquired from Thermo Fisher Scientific (Waltham, MA). Sodium acetate (3 M nuclease-free aqueous solution) was acquired from Thermo Fisher Scientific. 1,2-Distearoyl-*sn*-glycero-3-phosphocholine (DSPC), 1,2-distearoyl-*sn*-glycero-3-phospho-ethanolamine-*N*-[biotinyl(polyethylene glycol)-2000] (DSPE-PEG2000-Biotin), distearoyl-*rac*-glycero-3-methoxy (polyethylene glycol)-2000]) (DSG-PEG2000), and dimyristoyl-*rac*-glycero-3-methoxy (polyethylene glycol)-2000]) (DMG-PEG2000) were acquired from Avanti Polar Lipids (Alabaster, AL). Cholesterol was acquired from Lipoid (Ludwigshafen, Germany). (6Z,9Z,28Z,31Z)-Heptatriaconta-6,9,28,31-tetraen-19-yl 4-(dimethylamino)butanoate (DLin-MC3-DMA) was acquired from MedChemExpress (Monmouth Junction, NJ). 1,1′-Dioctadecyl-3,3,3′,3′-tetramethyl-indo-di-carbocyanine-5,5′-disulfonic acid (DiIC18(5)-DS, in this manuscript referred to as DiI) was acquired from Thermo Fisher Scientific (catalog no. D12730). The excitation/emission spectra of this fluorophore share more similarity with the lipophilic dye DiD than with conventional DiI. AF488-labeled anti-IgM (goat anti-mouse IgM [heavy chain] cross-adsorbed secondary antibody, catalog no. A-21042) and anti-IgG (goat anti-mouse IgG (H+L) cross-adsorbed secondary antibody, catalog no. A-11001) was acquired from Thermo Fisher Scientific. The anti-IgM antibody is specific to the mu chain of IgM and therefore only binds IgM antibodies according to the manufacturer. As the anti-IgG antibody is generated against whole IgG, there is a probability that it can cross-react with kappa and lambda chains of IgM, contributing to part the overall measured IgG signal. BSA, BSA-Biotin, and streptavidin for the SPAM assay were acquired from Sigma-Aldrich.

LNP preparation

LNPs were prepared using a microfluidic mixing method. In brief, lipids in powder forms were dissolved in ethanol, and the lipid stocks were mixed to achieve the desired final molar ratio. LNPs for injections consisted of DLin-MC3-DMA, cholesterol, DSPC, and DMG-PEG at a molar ratio of 50:38.5:10:1.5, with an N/P ratio 5 (30 nmol lipid per μg mRNA). In this study, the capturing LNPs used in the SPAM assay had a comparable composition and characteristics to the LNPs dosed in the animals, apart from the DMG-PEG2000 lipid being replaced with DSG-PEG2000 to eliminate PEG shedding during the plasma incubation of the LNPs and thereby simplifying the kinetics in the experiment. Also, 0.1 mol % DSPE-PEG2000-Biotin was added to the SPAM formulation for immobilization, and 0.5mol % DiI was added for imaging.

The lipid mixture was diluted in ethanol to a final concentration of 24 mM total lipid, and the mRNA stock was diluted in sodium acetate buffer (25 mM [pH 4.0]) to a final concentration of 200 μg/mL. The ethanol phase and aqueous phase were mixed in a 1:3 ratio at a total flow rate of 9 mL/min using a NanoAssemblr Ignite microfluidic mixer from Precision Nanosystems, equipped with a NxGen mixing cartridge. The buffer was exchanged to HEPES-buffered saline (HBS) (25 mM HEPES 150 mM NaCl [pH 7.4]) by discontinuous diafiltration. Specifically, this was done by transferring the LNP stock to Amicon Ultracel 4 (100 kDa MWCO) spin filtration columns (Merck) and diluting the LNPs 1:1 in HBS. The LNP stock was then upconcentrated $\times 2$ by centrifuging at $500 \times g$ at 22°C for 5–10 min. Six such 1:1 diafiltration steps were performed. In the final step, the volume was reduced to 200 μL, thus achieving a final concentration of approximately 500 μg/mL mRNA. The mRNA concentration was determined by disassembling the LNPs by incubating for 30 min at 60°C in 0.5% Triton X-100, and measuring the mRNA using the Quant-iT RiboGreen kit (Thermo Fisher Scientific) according to the manufacturer's instructions. Fluorescence of the RiboGreen dye was measured using a TECAN Spark microplate reader (Tecan, Männedorf, Switzerland). Encapsulation efficiency was determined by comparing the RNA concentration in disassembled LNPs to the RNA concentration in LNPs not being disassembled as described above. The hydrodynamic diameter and polydispersity index of the LNPs were measured by dynamic light scattering using a ZetaSizer Nano ZS from Malvern Instruments (Malvern, Worcestershire, UK), equipped with a 633 nm laser. The LNPs were diluted to about 6 μg/mL mRNA in HBS, and the size measured as the average from 3 runs of 15 cycles.

Animal experiments

Experimental work was carried out using 12-week-old female C57BL6/JRj mice obtained from Janvier Labs (Le Genest-Saint-Isle, France) and conducted at the Technical University of Denmark. Mice were subjected to at least 1 week of acclimation upon arrival and were kept under controlled environmental conditions (constant temperature, humidity, and 12:12 h light/dark cycle). All experimental procedures were approved by the institutional ethical board and the Danish National Animal Experiment Inspectorate. For intravenous injections, LNPs (total volume 100 μL, final concentration 60 μg/mL mRNA for the high dose and 0.06 μg/mL for the low dose) were injected into the tail vein. For subcutaneous injections, LNPs (total volume 100 μL, final concentration 60 μg/mL mRNA for the high dose and 0.06 μg/mL for the low dose) were injected in the neck. For intramuscular injections, LNPs (total volume 50 μL,

final concentration 120 μg/mL mRNA for the hgih dose and 0.12 μg/mL for the low dose) were injected into the thigh (biceps femuris). Sublingual blood was drawn 7 days after treatment in tubes containing 5–15 mM EDTA (concentration including blood volume). Plasma was obtained after centrifugation (1,500 × *g*, 15 min, 4°C). Resulting plasma fractions were collected in Protein LoBind Eppendorf tubes (Eppendorf, Hamburg, Germany) and stored at −80°C until SPAM analysis.

SPAM assay

To image individual LNPs we followed previously published protocols[31,64–67] used for tethering single liposomes onto passivated glass surfaces and imaging them using confocal microscopy. In brief, each chamber in an Ibidi μ-slide 8-well glass coverslip for microscopy (Ibidi, Martinsreid, Germany) was incubated with a 1 mg/mL 1:10 mixture of BSA-Biotin:BSA for 20 min at room temperature. After washing eight times with HEPES buffer, each chamber was incubated with 25 μg/mL streptavidin for 10 min, followed by eight additional washes with HEPES buffer. LNPs were diluted to a final concentration of 1 μM lipid and added to chambers on the coverslip. Unbound LNPs were removed by washing the plate in HEPES buffer after incubating for 3 min.

Next, plasma was diluted 1:20 in HEPES buffer, added to the well, and allowed to incubate with the immobilized LNPs for 10 min. Following two washes with HEPES buffer, secondary AF488-labeled antibodies against the respective antibody of interest (mouse IgG or IgM) were diluted to 1 μg/mL and added to the well. IgG binding was assessed using goat anti-mouse IgG (H+L) cross-adsorbed secondary antibody (Invitrogen) while IgM binding was assessed using goat anti-mouse IgM (heavy chain) cross-adsorbed secondary antibody (Invitrogen). With six fluorophores per antibody according to the manufacturer, single antibodies should be possible to detect. After an additional 10 min of incubation, unbound antibodies were removed by exchanging with fresh buffer before imaging the LNPs and detection antibodies.

For imaging LNPs we used a Nikon Ti2, Yokogawa CSU-W1 spinning disc confocal microscope equipped with a 100× oil immersion CFI Plan Apochromat Lambda NA 1.45 objective and a Photometrics Prime 95B sCMOS detector. The DiI (LNP) channel was acquired using 500 ms exposure by a 640 nm excitation laser and detection through a 700/75 ET band-pass filter. The ALA AF488 (ALA) channel was acquired sequentially by using 500 ms exposure by a 488 nm laser excitation and detection through a 520/28 BrightlLine HC band-pass filter. Data were analyzed using custom-made routines in Igor Pro (Wavemetrics) allowing for automated spot detection and 2D Gauss fitting to individual diffraction limited intensity spots to extract the integrated intensity for both the DiI (LNP) and AF488 (ALA) channels for each individual LNP. Data treatment was done using Excel. Statistical analysis was performed in GraphPad Prism.

DATA AVAILABILITY

The data that support the findings of this study are available from the corresponding author, Jannik B. Larsen, upon reasonable request.

SUPPLEMENTAL INFORMATION

Supplemental information can be found online at https://doi.org/10.1016/j.omtm.2023.05.008.

ACKNOWLEDGMENTS

This work was supported by the Novo Nordisk Foundation grant no. NNF16OC0022166. The funding source was not involved in any part of the study design, data collection, data analysis, interpretation of the data, or the writing of the manuscript.

AUTHOR CONTRIBUTIONS

All authors were involved in conceiving the study and designing the experimental setup. R.M. formulated and characterized the LNPs. E.C. carried out the *in vivo* experiments. J.B.L. performed the microscopy and the data analysis. All authors were involved in interpretation of the results. R.M. and J.B.L wrote the first draft of the manuscript. T.L.A. supervised the study. All authors corrected and approved the manuscript.

DECLARATION OF INTERESTS

T.L.A. is an employee of T Cypher Bio.

REFERENCES

1. de Lázaro, I., and Mooney, D.J. (2021). Obstacles and opportunities in a forward vision for cancer nanomedicine. Nat. Mater. *20*, 1469–1479. https://doi.org/10.1038/s41563-021-01047-7.

2. Koide, H., Asai, T., Hatanaka, K., Akai, S., Ishii, T., Kenjo, E., Ishida, T., Kiwada, H., Tsukada, H., and Oku, N. (2010). T cell-independent B cell response is responsible for ABC phenomenon induced by repeated injection of PEGylated liposomes. Int. J. Pharm. *392*, 218–223. https://doi.org/10.1016/j.ijpharm.2010.03.022.

3. Barbier, A.J., Jiang, A.Y., Zhang, P., Wooster, R., and Anderson, D.G. (2022). The clinical progress of mRNA vaccines and immunotherapies. Nat. Biotechnol. *40*, 840–854. https://doi.org/10.1038/s41587-022-01294-2.

4. Damase, T.R., Sukhovershin, R., Boada, C., Taraballi, F., Pettigrew, R.I., and Cooke, J.P. (2021). The limitless future of RNA therapeutics. Front. Bioeng. Biotechnol. *9*, 628137. https://doi.org/10.3389/fbioe.2021.628137.

5. Verma, M., Ozer, I., Xie, W., Gallagher, R., Teixeira, A., and Choy, M. (2023). The landscape for lipid-nanoparticle-based genomic medicines. Nat. Rev. Drug Discov. *22*, 349–350. https://doi.org/10.1038/d41573-023-00002-2.

6. Rohner, E., Yang, R., Foo, K.S., Goedel, A., and Chien, K.R. (2022). Unlocking the promise of mRNA therapeutics. Nat. Biotechnol. *40*, 1586–1600. https://doi.org/10.1038/s41587-022-01491-z.

7. Kulkarni, J.A., Witzigmann, D., Thomson, S.B., Chen, S., Leavitt, B.R., Cullis, P.R., and van der Meel, R. (2021). The current landscape of nucleic acid therapeutics. Nat. Nanotechnol. *16*, 630–643. https://doi.org/10.1038/s41565-021-00898-0.

8. Anselmo, A.C., and Mitragotri, S. (2021). Nanoparticles in the clinic: an update post COVID -19 vaccines. Bioeng. Transl. Med. *6*, e10246. https://doi.org/10.1002/btm2.10246.

9. Witzigmann, D., Kulkarni, J.A., Leung, J., Chen, S., Cullis, P.R., and van der Meel, R. (2020). Lipid nanoparticle technology for therapeutic gene regulation in the liver. Adv. Drug Deliv. Rev. *159*, 344–363. https://doi.org/10.1016/j.addr.2020.06.026.

10. Akinc, A., Maier, M.A., Manoharan, M., Fitzgerald, K., Jayaraman, M., Barros, S., Ansell, S., Du, X., Hope, M.J., Madden, T.D., et al. (2019). The Onpattro story and the clinical translation of nanomedicines containing nucleic acid-based drugs. Nat. Nanotechnol. *14*, 1084–1087. https://doi.org/10.1038/s41565-019-0591-y.

11. Chaudhary, N., Weissman, D., and Whitehead, K.A. (2021). mRNA vaccines for infectious diseases: principles, delivery and clinical translation. Nat. Rev. Drug Discov. *20*, 817–838. https://doi.org/10.1038/s41573-021-00283-5.

12. Heine, A., Juranek, S., and Brossart, P. (2021). Clinical and immunological effects of mRNA vaccines in malignant diseases. Mol. Cancer *20*, 52. https://doi.org/10.1186/s12943-021-01339-1.

13. Moghimi, S.M. (2021). Allergic reactions and anaphylaxis to LNP-based COVID-19 vaccines. Mol. Ther. *29*, 898–900. https://doi.org/10.1016/j.ymthe.2021.01.030.

14. Szebeni, J., Storm, G., Ljubimova, J.Y., Castells, M., Phillips, E.J., Turjeman, K., Barenholz, Y., Crommelin, D.J.A., and Dobrovolskaia, M.A. (2022). Applying lessons learned from nanomedicines to understand rare hypersensitivity reactions to mRNA-based SARS-CoV-2 vaccines. Nat. Nanotechnol. *17*, 337–346. https://doi.org/10.1038/s41565-022-01071-x.

15. Bigini, P., Gobbi, M., Bonati, M., Clavenna, A., Zucchetti, M., Garattini, S., and Pasut, G. (2021). The role and impact of polyethylene glycol on anaphylactic reactions to COVID-19 nano-vaccines. Nat. Nanotechnol. *16*, 1169–1171. https://doi.org/10.1038/s41565-021-01001-3.

16. Schreiner, M., Zobel, C., Baumgarten, U., Uhlmann, T., and Vandersee, S. (2022). Anaphylactic reactions to polyethylene glycol-containing bowel cleansing preparations after Moderna COVID-19 vaccination. Endoscopy *54*, 517–518. https://doi.org/10.1055/a-1640-9686.

17. Chen, B.M., Cheng, T.L., and Roffler, S.R. (2021). Polyethylene glycol immunogenicity: theoretical, clinical, and practical aspects of anti-polyethylene glycol antibodies. ACS Nano *15*, 14022–14048. https://doi.org/10.1021/acsnano.1c05922.

18. Suzuki, T., Suzuki, Y., Hihara, T., Kubara, K., Kondo, K., Hyodo, K., Yamazaki, K., Ishida, T., and Ishihara, H. (2020). PEG shedding-rate-dependent blood clearance of PEGylated lipid nanoparticles in mice: faster PEG shedding attenuates anti-PEG IgM production. Int. J. Pharm. *588*, 119792. https://doi.org/10.1016/j.ijpharm.2020.119792.

19. Mohamed, M., Abu Lila, A.S., Shimizu, T., Alaaeldin, E., Hussein, A., Sarhan, H.A., Szebeni, J., and Ishida, T. (2019). PEGylated liposomes: immunological responses. Sci. Technol. Adv. Mater. *20*, 710–724. https://doi.org/10.1080/14686996.2019.1627174.

20. Szebeni, J., Simberg, D., González-Fernández, Á., Barenholz, Y., and Dobrovolskaia, M.A. (2018). Roadmap and strategy for overcoming infusion reactions to nanomedicines. Nat. Nanotechnol. *13*, 1100–1108. https://doi.org/10.1038/s41565-018-0273-1.

21. Stavnsbjerg, C., Christensen, E., Münter, R., Henriksen, J.R., Fach, M., Parhamifar, L., Christensen, C., Kjaer, A., Hansen, A.E., and Andresen, T.L. (2022). Accelerated blood clearance and hypersensitivity by PEGylated liposomes containing TLR agonists. J. Contr. Release *342*, 337–344. https://doi.org/10.1016/j.jconrel.2021.12.033.

22. Kozma, G.T., Shimizu, T., Ishida, T., and Szebeni, J. (2020). Anti-PEG antibodies: properties, formation, testing and role in adverse immune reactions to PEGylated nano-biopharmaceuticals. Adv. Drug Deliv. Rev. *154-155*, 163–175. https://doi.org/10.1016/j.addr.2020.07.024.

23. Freire Haddad, H., Burke, J.A., Scott, E.A., and Ameer, G.A. (2022). Clinical relevance of pre-existing and treatment-induced anti-poly(ethylene glycol) antibodies. Regen. Eng. Transl. Med. *8*, 32–42. https://doi.org/10.1007/s40883-021-00198-y.

24. Valsecchi, C., Gualtierotti, R., Arcudi, S., Ciavarella, A., Schiavone, L., Novembrino, C., Siboni, S.M., Mannucci, P.M., and Peyvandi, F. (2023). Reduced FVIII recovery associated with anti-FVIII PEG antibodies after BNT162b2 SARS-CoV-2 vaccination. Blood Adv. *7*, 174–177. https://doi.org/10.1182/BLOODADVANCES.2022008989.

25. Besin, G., Milton, J., Sabnis, S., Howell, R., Mihai, C., Burke, K., Benenato, K.E., Stanton, M., Smith, P., Senn, J., et al. (2019). Accelerated blood clearance of lipid nanoparticles entails a biphasic humoral response of B-1 followed by B-2 lymphocytes to distinct antigenic moieties. Immunohorizons *3*, 282–293. https://doi.org/10.4049/IMMUNOHORIZONS.1900029/-/DCSUPPLEMENTAL.

26. Ju, Y., Lee, W.S., Pilkington, E.H., Kelly, H.G., Li, S., Selva, K.J., Wragg, K.M., Subbarao, K., Nguyen, T.H.O., Rowntree, L.C., et al. (2022). Anti-PEG antibodies boosted in humans by SARS-CoV-2 lipid nanoparticle mRNA vaccine. ACS Nano *16*, 11769–11780. https://doi.org/10.1021/acsnano.2c04543.

27. Carreño, J.M., Singh, G., Tcheou, J., Srivastava, K., Gleason, C., Muramatsu, H., Desai, P., Aberg, J.A., Miller, R.L., Pardi, N., et al. (2022). mRNA-1273 but not BNT162b2 induces antibodies against polyethylene glycol (PEG) contained in mRNA-based vaccine formulations. medRxiv *40*, 2022. https://doi.org/10.1101/2022.04.15.22273914.

28. Guerrini, G., Gioria, S., Sauer, A.v., Lucchesi, S., Montagnani, F., Pastore, G., Ciabattini, A., Medaglini, D., and Calzolai, L. (2022). Monitoring anti-PEG antibodies level upon repeated lipid nanoparticle-based COVID-19 vaccine administration. Int. J. Mol. Sci. *23*, 8838.23. https://doi.org/10.3390/IJMS23168838.

29. Bavli, Y., Chen, B.M., Gross, G., Hershko, A., Turjeman, K., Roffler, S., and Barenholz, Y. (2023). Anti-PEG antibodies before and after a first dose of Comirnaty® (mRNA-LNP-based SARS-CoV-2 vaccine). J. Contr. Release *354*, 316–322. https://doi.org/10.1016/J.JCONREL.2022.12.039.

30. Münter, R., Sørensen, E., Hasselbalch, R.B., Christensen, E., Nielsen, S.D., Garred, P., Ostrowski, S.R., Bundgaard, H., Iversen, K.K., Andresen, T.L., et al. (2023). Investigating generation of antibodies against the lipid nanoparticle vector following COVID-19 vaccination with an mRNA vaccine. Preprint at Mol. Pharm. https://doi.org/10.1021/ACS.MOLPHARMACEUT.2C01036.

31. Münter, R., Stavnsbjerg, C., Christensen, E., Thomsen, M.E., Stensballe, A., Hansen, A.E., Parhamifar, L., Kristensen, K., Simonsen, J.B., Larsen, J.B., et al. (2022). Unravelling heterogeneities in complement and antibody opsonization of individual liposomes as a function of surface architecture. Small *18*, 2106529. https://doi.org/10.1002/smll.202106529.

32. Ishida, T., Harada, M., Wang, X.Y., Ichihara, M., Irimura, K., and Kiwada, H. (2005). Accelerated blood clearance of PEGylated liposomes following preceding liposome injection: effects of lipid dose and PEG surface-density and chain length of the first-dose liposomes. J. Contr. Release *105*, 305–317. https://doi.org/10.1016/j.jconrel.2005.04.003.

33. Davies, N., Hovdal, D., Edmunds, N., Nordberg, P., Dahlén, A., Dabkowska, A., Arteta, M.Y., Radulescu, A., Kjellman, T., Höijer, A., et al. (2021). Functionalized lipid nanoparticles for subcutaneous administration of mRNA to achieve systemic exposures of a therapeutic protein. Mol. Ther. Nucleic Acids *24*, 369–384. https://doi.org/10.1016/j.omtn.2021.03.008.

34. Mima, Y., Abu Lila, A.S., Shimizu, T., Ukawa, M., Ando, H., Kurata, Y., and Ishida, T. (2017). Ganglioside inserted into PEGylated liposome attenuates anti-PEG immunity. J. Contr. Release *250*, 20–26. https://doi.org/10.1016/j.jconrel.2017.01.040.

35. Judge, A., McClintock, K., Phelps, J.R., and MacLachlan, I. (2006). Hypersensitivity and loss of disease site targeting caused by antibody responses to PEGylated liposomes. Mol. Ther. *13*, 328–337. https://doi.org/10.1016/j.ymthe.2005.09.014.

36. Ishida, T., Wang, X., Shimizu, T., Nawata, K., and Kiwada, H. (2007). PEGylated liposomes elicit an anti-PEG IgM response in a T cell-independent manner. J. Contr. Release *122*, 349–355. https://doi.org/10.1016/j.jconrel.2007.05.015.

37. Grenier, P., Chénard, V., and Bertrand, N. (2023). The mechanisms of anti-PEG immune response are different in the spleen and the lymph nodes. J. Contr. Release *353*, 611–620. https://doi.org/10.1016/J.JCONREL.2022.12.005.

38. Kozma, G.T., Mészáros, T., Vashegyi, I., Fülöp, T., Örfi, E., Dézsi, L., Rosivall, L., Bavli, Y., Urbanics, R., Mollnes, T.E., et al. (2019). Pseudo-anaphylaxis to polyethylene glycol (PEG)-Coated liposomes: roles of anti-PEG IgM and complement activation in a porcine model of human infusion reactions. ACS Nano *13*, 9315–9324. https://doi.org/10.1021/acsnano.9b03942.

39. Rabanel, J.-M., Adibnia, V., Tehrani, S.F., Sanche, S., Hildgen, P., Banquy, X., and Ramassamy, C. (2019). Nanoparticle heterogeneity: an emerging structural parameter influencing particle fate in biological media? Nanoscale *11*, 383–406. https://doi.org/10.1039/C8NR04916E.

40. Forest, V., and Pourchez, J. (2016). The nanoparticle protein corona: the myth of average. Nano Today *11*, 700–703. https://doi.org/10.1016/j.nantod.2015.10.007.

41. Kristensen, K., Engel, T.B., Stensballe, A., Simonsen, J.B., and Andresen, T.L. (2019). The hard protein corona of stealth liposomes is sparse. J. Contr. Release *307*, 1–15. https://doi.org/10.1016/j.jconrel.2019.05.042.

42. Kristensen, K., Münter, R., Kempen, P.J., Thomsen, M.E., Stensballe, A., and Andresen, T.L. (2021). Isolation methods commonly used to study the liposomal protein corona suffer from contamination issues. Acta Biomater. *130*, 460–472. https://doi.org/10.1016/j.actbio.2021.06.008.

43. Simonsen, J.B., and Münter, R. (2020). Pay attention to biological nanoparticles when studying the protein corona on nanomedicines. Angew. Chem., Int. Ed. Engl. *59*, 12584–12588. https://doi.org/10.1002/anie.202004611.

44. Münter, R., and Simonsen, J.B. (2023). Comment on "Optimal centrifugal isolating of liposome–protein complexes from human plasma" by L. Digiacomo, F. Giulimondi,

A. L. Capriotti, S. Piovesana, C. M. Montone, R. Z. Chiozzi, A. Laganá, M. Mahmoudi, D. Pozzi and G. Caracciolo, Nanoscale Adv. , 2021, 3 , 3824. Nanoscale Adv. *5*, 290–299. https://doi.org/10.1039/D2NA00343K.

45. Miao, L., Lin, J., Huang, Y., Li, L., Delcassian, D., Ge, Y., Shi, Y., and Anderson, D.G. (2020). Synergistic lipid compositions for albumin receptor mediated delivery of mRNA to the liver. Nat. Commun. *11*, 2424. https://doi.org/10.1038/s41467-020-16248-y.

46. Rybakova, Y., Kowalski, P.S., Huang, Y., Gonzalez, J.T., Heartlein, M.W., DeRosa, F., Delcassian, D., and Anderson, D.G. (2019). mRNA delivery for therapeutic anti-HER2 antibody expression in vivo. Mol. Ther. *27*, 1415–1423. https://doi.org/10.1016/j.ymthe.2019.05.012.

47. Oberli, M.A., Reichmuth, A.M., Dorkin, J.R., Mitchell, M.J., Fenton, O.S., Jaklenec, A., Anderson, D.G., Langer, R., and Blankschtein, D. (2017). Lipid nanoparticle assisted mRNA delivery for potent cancer immunotherapy. Nano Lett. *17*, 1326–1335. https://doi.org/10.1021/acs.nanolett.6b03329.

48. Kauffman, K.J., Dorkin, J.R., Yang, J.H., Heartlein, M.W., DeRosa, F., Mir, F.F., Fenton, O.S., and Anderson, D.G. (2015). Optimization of lipid nanoparticle formulations for mRNA delivery in vivo with fractional factorial and definitive screening designs. Nano Lett. *15*, 7300–7306. https://doi.org/10.1021/acs.nanolett.5b02497.

49. Cheng, Q., Wei, T., Farbiak, L., Johnson, L.T., Dilliard, S.A., and Siegwart, D.J. (2020). Selective organ targeting (SORT) nanoparticles for tissue-specific mRNA delivery and CRISPR–Cas gene editing. Nat. Nanotechnol. *15*, 313–320. https://doi.org/10.1038/s41565-020-0669-6.

50. Feiner-Gracia, N., Beck, M., Pujals, S., Tosi, S., Mandal, T., Buske, C., Linden, M., and Albertazzi, L. (2017). Super-resolution microscopy unveils dynamic heterogeneities in nanoparticle protein corona. Small *13*, 1701631. https://doi.org/10.1002/smll.201701631.

51. Shimizu, T., Ishida, T., and Kiwada, H. (2013). Transport of PEGylated liposomes from the splenic marginal zone to the follicle in the induction phase of the accelerated blood clearance phenomenon. Immunobiology *218*, 725–732. https://doi.org/10.1016/j.imbio.2012.08.274.

52. Zahednezhad, F., Saadat, M., Valizadeh, H., Zakeri-Milani, P., and Baradaran, B. (2019). Liposome and immune system interplay: challenges and potentials. J. Contr. Release *305*, 194–209. https://doi.org/10.1016/j.jconrel.2019.05.030.

53. Copaescu, A.M., Rosa Duque, J.S., and Phillips, E.J. (2022). What have we learned about the allergenicity and adverse reactions associated with the severe acute respiratory syndrome coronavirus 2 vaccines: one year later. Ann. Allergy Asthma Immunol. *129*, 40–51. https://doi.org/10.1016/j.anai.2022.03.030.

54. Ju, Y., Carreño, J.M., You, M., Dawson, K., Krammer, F., and Kent, S.J. (2022). Impact of anti-PEG antibodies induced by SARS-CoV-2 mRNA vaccines. Health Commun. *2022*, 1–9. https://doi.org/10.1038/s41577-022-00825-x.

55. (1994). 4 - subcutaneous drug administration. In Neglected Factors in Pharmacology and Neuroscience Research Techniques in the Behavioral and Neural Sciences, V. Claassen, ed. (Elsevier), pp. 35–45. https://doi.org/10.1016/B978-0-444-81871-3.50009-6.

56. Di, J., Du, Z., Wu, K., Jin, S., Wang, X., Li, T., and Xu, Y. (2022). Biodistribution and non-linear gene expression of mRNA LNPs affected by delivery route and particle size. Pharm. Res. (N. Y.) *39*, 105–114. https://doi.org/10.1007/S11095-022-03166-5/FIGURES/6.

57. Münter, R., Kristensen, K., Pedersbæk, D., Andresen, T.L., Simonsen, J.B., and Larsen, J.B. (2019). Quantitative methods for investigating dissociation of fluorescently labeled lipids from drug delivery liposomes. In Nanotechnology Characterization Tools for Tissue Engineering and Medical Therapy (Springer Berlin Heidelberg), pp. 333–359. https://doi.org/10.1007/978-3-662-59596-1_8.

58. Zhu, X., Tao, W., Liu, D., Wu, J., Guo, Z., Ji, X., Bharwani, Z., Zhao, L., Zhao, X., Farokhzad, O.C., et al. (2017). Surface de-PEGylation controls nanoparticle-mediated siRNA delivery in vitro and in vivo. Theranostics *7*, 1990–2002. https://doi.org/10.7150/thno.18136.

59. Mui, B.L., Tam, Y.K., Jayaraman, M., Ansell, S.M., Du, X., Tam, Y.Y.C., Lin, P.J., Chen, S., Narayanannair, J.K., Rajeev, K.G., et al. (2013). Influence of polyethylene glycol lipid desorption rates on pharmacokinetics and pharmacodynamics of siRNA lipid nanoparticles. Mol. Ther. Nucleic Acids *2*, e139. https://doi.org/10.1038/mtna.2013.66.

60. Carrasco, M.J., Alishetty, S., Alameh, M.G., Said, H., Wright, L., Paige, M., Soliman, O., Weissman, D., Cleveland, T.E., Grishaev, A., and Buschmann, M.D. (2021). Ionization and structural properties of mRNA lipid nanoparticles influence expression in intramuscular and intravascular administration. Commun. Biol. *4*, 956. https://doi.org/10.1038/s42003-021-02441-2.

61. Mabrouk, M.T., Huang, W.C., Martinez-Sobrido, L., and Lovell, J.F. (2022). Advanced materials for SARS-CoV-2 vaccines. Adv. Mater. *34*, e2107781. https://doi.org/10.1002/adma.202107781.

62. Havenar-Daughton, C., Carnathan, D.G., Boopathy, A.V., Upadhyay, A.A., Murrell, B., Reiss, S.M., Enemuo, C.A., Gebru, E.H., Choe, Y., Dhadvai, P., et al. (2019). Rapid germinal center and antibody responses in non-human primates after a single nanoparticle vaccine immunization. Cell Rep. *29*, 1756–1766.e8. https://doi.org/10.1016/j.celrep.2019.10.008.

63. Cabanillas, B., Novak, N., and Akdis, C.A. (2022). The form of PEG matters: PEG conjugated with lipids and not PEG alone could be the specific form involved in allergic reactions to COVID-19 vaccines. Allergy *77*, 1658–1660. https://doi.org/10.1111/all.15187.

64. Münter, R., Andresen, T.L., and Larsen, J.B. (2019). A quantitative fluorescence microscopy-based single liposome assay for detecting the compositional inhomogeneity between individual liposomes. JoVE, e60538. https://doi.org/10.3791/60538.

65. Larsen, J., Hatzakis, N.S., and Stamou, D. (2011). Observation of inhomogeneity in the lipid composition of individual nanoscale liposomes. J. Am. Chem. Soc. *133*, 10685–10687. https://doi.org/10.1021/ja203984j.

66. Larsen, J.B., Jensen, M.B., Bhatia, V.K., Pedersen, S.L., Bjørnholm, T., Iversen, L., Uline, M., Szleifer, I., Jensen, K.J., Hatzakis, N.S., et al. (2015). Membrane curvature enables N-Ras lipid anchor sorting to liquid-ordered membrane phases. Nat. Chem. Biol. *11*, 192–194. https://doi.org/10.1038/nchembio.1733.

67. Hatzakis, N.S., Bhatia, V.K., Larsen, J., Madsen, K.L., Bolinger, P.-Y., Kunding, A.H., Castillo, J., Gether, U., Hedegård, P., and Stamou, D. (2009). How curved membranes recruit amphipathic helices and protein anchoring motifs. Nat. Chem. Biol. *5*, 835–841. https://doi.org/10.1038/nchembio.213.